Original Article

High-fat diet causes mitochondrial damage and downregulation of mitofusin-2 and optic atrophy-1 in multiple organs

Peng Zheng,[1,†] Wenjing Ma,[2,†] Yilu Gu,[3] Hengfang Wu,[1] Zhiping Bian,[1] Nannan Liu,[1] Di Yang,[1,2,*] and Xiangjian Chen[1,*]

[1]Department of Cardiology, [2]Core Facility, and [3]Department of Pathology, The First Affiliated Hospital of Nanjing Medical University, 300 Guangzhou Road, Nanjing 210029, Jiangsu, China

(Received 1 July, 2022; Accepted 19 February, 2023; Released online in J-STAGE as advance publication 25 May, 2023)

High-fat consumption promotes the development of obesity, which is associated with various chronic illnesses. Mitochondria are the energy factories of eukaryotic cells, maintaining self-stability through a fine-tuned quality-control network. In the present study, we evaluated high-fat diet (HFD)-induced changes in mitochondrial ultrastructure and dynamics protein expression in multiple organs. C57BL/6J male mice were fed HFD or normal diet (ND) for 24 weeks. Compared with ND-fed mice, HFD-fed mice exhibited increased body weight, cardiomyocyte enlargement, pulmonary fibrosis, hepatic steatosis, renal and splenic structural abnormalities. The cellular apoptosis of the heart, liver, and kidney increased. Cellular lipid droplet deposition and mitochondrial deformations were observed. The proteins related to mitochondrial biogenesis (TFAM), fission (DRP1), autophagy (LC3 and LC3-II: LC3-I ratio), and mitophagy (PINK1) presented different changes in different organs. The mitochondrial fusion regulators mitofusin-2 (MFN2) and optic atrophy-1 (OPA1) were consistently downregulated in multiple organs, even the spleen. TOMM20 and ATP5A protein were enhanced in the heart, skeletal muscle, and spleen, and attenuated in the kidney. These results indicated that high-fat feeding caused pathological changes in multiple organs, accompanied by mitochondrial ultrastructural damage, and MFN2 and OPA1 downregulation. The mitochondrial fusion proteins may become promising targets and/or markers for treating metabolic disease.

***Key Words*:** **high-fat diet, hyperlipidemia, mitochondria, mitofusin-2, optic atrophy-1**

Epidemiological studies have shown a significant positive relationship between the average amount of fat in the diet and the incidence of obesity.[1] Obesity is closely correlated with various diseases and conditions, particularly cardiovascular disease, type 2 diabetes, non-alcoholic hepatic steatosis, renal disease, mental health problems, and certain malignancies.[2] Its prevalence exhibits a continuous increase and has doubled worldwide during the past thirty-five years.[3] Mitochondria are the energy factories of eukaryotic cells, provide ATP through oxidative phosphorylation (OXPHOS), and participate in regulating crucial cellular physiological processes.[4] Mitochondria maintain their dynamics homeostasis through mitophagy, biogenesis, fission, and fusion processes that are involved in various delicate proteins.[5] Mitochondrial dynamics is essential for regulating cell number, morphology, function, and subcellular distribution.[6] Defective mitochondria are involved in the pathophysiological progression of various diseases.[7] The effects of a high-fat diet (HFD) on mitochondria are complex. HFD can be both beneficial and detrimental to the mitochondrion.[8] HFD has been shown to improve mitochondrial function and/or density, reduce the mitochondrial bioenergetics in skeletal muscle and liver,[9,10] and enhance the mitochondrial fatty acid oxidation rate in the heart.[11] The duration of treatment may determine the observed effects of HFD. However, the effects of chronic high-fat consumption on mitochondrial dynamics aren't fully clarified.

We presumed that the impairments of mitochondrial structure and dynamics homeostasis are shared alterations accounting for multiple organ complications caused by HFD feeding, when pathological tissue changes in multiple organs. In the present study, we systemically evaluated the pathological changes, mitochondrial ultrastructural damage, and mitochondrial dynamics protein expression of multiple organs in C57BL/6J male mice fed HFD for 24 weeks.

Materials and Methods

Animals. C57BL/6J male mice (four-week-old, average body weight: 15 g) were obtained from the Animal Core Facility of Nanjing Medical University. Only male mice were used in this study to avoid the impact of sex hormones on the experimental outcomes. All mice were housed in a 20–26°C environment with a 12/12 h light/dark photoperiod and were given free access to food and water. After one week of environmental adaptation, the mice were randomly divided into two groups to be fed a normal diet (ND, 12 kcal% fat, 23 kcal% protein, and 65 kcal% carbohydrate; KeAo XieLi, Beijing, China, $n = 5$) or a HFD (D12492, 60 kcal% fat, 20 kcal% protein, and 20 kcal% carbohydrate; Research Diets, Inc., New Brunswick, NJ, $n = 9$) for 24 weeks. This study was approved and supervised by the Institutional Animal Care and Use Committee of Nanjing Medical University (IACUC1708009). All methods were performed in accordance with the relevant guidelines and regulations. All methods are reported in accordance with the ARRIVE guidelines.

Biochemistry assay and organ collection. Mice were fasted for 12 h before their body weights were measured. The blood was collected through retro-orbital bleeding after the mice were anesthetized with isoflurane inhalation. The serum total cholesterol (TC), triglyceride (TG), high- or low-density lipoprotein cholesterol (HDL-C or LDL-C), glucose, alanine aminotransferase (ALT), and aspartate aminotransferase (AST) levels were determined by an automatic biochemistry analyzer

[†]These authors contributed equally to this work.
*To whom correspondence should be addressed.
E-mail: diyang@njmu.edu.cn (DY), chenxiangjian@njmu.edu.cn (XC)

doi: 10.3164/jcbn.22-73

(Beckman Coulte, Brea, CA).

The heart, lung, thoracic aorta, liver, kidney, spleen, and skeletal muscle (quadriceps femoris) of mice were instantly dissected at sacrifice and rinsed with a pre-cooled phosphate buffered solution (PBS, pH 7.40). The heart, liver, right kidney, and spleen were weighted, respectively. The body weight gain was defined as the difference between the final and initial body weights. The ratio of internal organ weight to body weight was calculated. The tissue was either quickly frozen in liquid nitrogen for the subsequent immunoblotting or fixed and embedded for histochemistry or transmission electron microscopy analysis.

Histochemistry. Fresh tissue was fixed with 4% paraformaldehyde overnight, dehydrated with gradient ethanol, embedded in paraffin, and sectioned for hematoxylin and eosin (HE), Masson's trichrome, and periodic acid-schiff (PAS) staining. The cardiomyocyte size was obtained by averaging the data of 30 to 45 cardiomyocytes from three different regions of the left ventricle per section from no less than three mice in each group using ImageJ software. The kidney injury score was calculated according to the previous study.[12] The semi-quantitative scale was classified from 0 to 4 (0, normal kidney; 1, 0–5%, minimal injury; 2, 5–25%, mild injury; 3, 25–75%, moderate injury; 4, 75–100%, severe injury). The sliders were photographed using an Aperio CS2 image capture device (Leica, Hamburg, Germany), and 4 to 6 high-resolution fields per section from no less than three mice in each group were randomly selected to perform semi-quantitative analysis by Image-Pro Plus software 6.0 (IPP 6.0). The collagen and glycogen content of multiple tissues in the HFD group were normalized by those in the ND group.

Transmission electron microscopy. Fresh heart, skeletal muscle, liver, and kidney tissues were cut into 1 mm^3 and fixed with 5% glutaraldehyde overnight. Secondary fixation was subsequently executed with 1% osmium tetroxide. After being dehydrated by an ethanol series and acetone at 4°C, the fixed tissues were embedded in epoxy resin. Eventually, the ultrathin continuous sections (60 nm) from the embedded tissues were stained by lead citrate and uranyl acetate and observed under transmission electron microscopy (TEM) at an acceleration of 80 kV (TEM, TecnaiTM G2 Spirit BioTWIN; FEI, Hillsboro, OR).

Cellular apoptosis assay. Cellular apoptosis was determined by terminal deoxynucleotidyl transferase (TdT) dUTP nick end labeling (TUNEL) staining with paraffin-embedded tissues according to the manufacturer's instructions (MK1015; Boster Biological Technology, Wuhan, China). The images were photographed, and positive cells in five high-resolution fields per section from no less than three mice per group were calculated by IPP 6.0 software program.

Immunohistochemistry. The paraffin-embedded sections (4 μm) were deparaffinized by xylene and rehydrated by gradient ethanol. Hydrogen peroxide (0.3%) and bovine serum albumin (5%) were used to block the endogenous enzymes and non-specific antigen, respectively. The sections were incubated with the primary antibodies at 4°C overnight and then with the secondary antibodies (KIT5001 or KIT5005; MXB Biotechnologies Company, Fuzhou, China) at room temperature for 30 min. The sections were photographed, and 4 to 6 high-resolution fields per section from no less than three mice per group were randomly selected to perform semi-quantitative analysis by IPP 6.0 software. The primary antibodies against the α-smooth muscle actin (α-SMA, #19245, 1:500; Cell Signaling Technology, Beverly, MA) which typically expressed in the vascular smooth muscle, a mitochondrial fission regulator dynamin-related protein 1 (DRP1, ab184247, 1:500 in kidney tissue or 1:1,600 in muscle tissue; Abcam, Cambridge, UK), a key protein for mitochondrial fusion mitofusin-2 (MFN2, ab56889 used for kidney tissue, 1:200; Abcam; 12186-1-AP used for heart and skeletal muscle tissue, 1:400; Proteintech, Rosemont, IL), a key autophagy regulator microtubule-associated protein 1A/1B-light chain 3 (LC3, 14600-1-AP, 1:400; Proteintech), a core mitochondrial transcription factor A (TFAM, 18836-1-AP, 1:100; Proteintech), were used in this study.

Immunoblotting. Total protein was extracted using RIPA buffer (Beyotime, China), separated by 10% SDS-PAGE, and transferred to PVDF membranes (Millipore, Billerica, MA). Then, the blots were incubated with the primary antibodies against DRP1 (1:1,000, ab184247; Abcam), LC3 (1:1,000, ab48394; Abcam), mitofusin-1 (MFN1, 1:800, 13798-1-AP; Proteintech), MFN2 (1:2,000, 12186-1-AP; Proteintech), optic atrophy-1 (OPA1, 1:1,000, DF8575; Affinity, Cincinnati, OH), TFAM (1:1,000, AF0531; Affinity), PTEN induced kinase 1 (PINK1, 1:1,000, DF7742; Affinity), mitochondrial import receptor subunit TOM20 homolog (TOMM20, 1:5,000, 11802-1-AP; Proteintech), ATP synthase subunit α (ATP5A, 1:2,000, 14676-1-AP; Proteintech), GAPDH (1:7,500, #21612; Signalway Antibody LCC, Greenbelt, MD), and tubulin (1:2,500, AF7011; Affinity) at 4°C overnight and horseradish peroxidase (HRP)-conjugated secondary antibody (ab6721, 1:15,000; Abcam). Signals were detected by ECL and quantified by a Multi Tanon 5200 imaging system. The tubulin or GAPDH was used as internal control. Protein levels were expressed as relative to Tubulin or GAPDH. The LC3-II:LC3-I ratio was calculated based on densitometry analysis of both bands.

Statistical analysis. Data are presented as mean ± SD. Unpaired *t* test was used to detect statistical differences between both groups with GraphPad 7.0. $P<0.05$ represented a significant difference.

Results

High-fat feeding induced obesity and hyperlipidemia in mice. The studies from humans and animals reveal that obesity is positively associated with fat dietary intake, and diets containing more than 30% of total energy from fat may easily develop obesity.[1] We first verified that the increased body weight responded to high-fat consumption. In the initial 12 weeks of feeding, the body weights of mice in both ND-fed and HFD-fed groups increased gradually, and there was no significant difference between the two groups (Fig. 1A). A significant difference in body weight between HFD-fed and ND-fed mice was observed at 16–24 weeks (48.08 ± 3.88 g vs 31.88 ± 1.45 g at the end of the 24th feeding, $p<0.01$; Fig. 1A). High-fat feeding resulted in greater body weight gain (31.98 ± 4.61 g vs 16.62 ± 1.78 g, $p<0.01$). It suggested that during the initial feeding, body weight gain in mice was largely related to maturation. Since 12-week-old age, the body weight of ND-fed mice remained basically stable, and high-fat consumption became a major contributor to body weight gain and eventually induced dietary obesity. The four internal organs were weighted at the end of the experiment. We found that the weights of the heart, liver, and spleen in HFD-fed mice were higher than in ND-fed mice, and only the changes in spleen weight presented a statistical difference ($p<0.01$) (Fig. 1B–E). There was no difference in kidney weight between HFD- and ND-fed mice ($p>0.05$, Fig. 1D). The increments of heart, liver, and spleen weight contributed to 0.038%, 2.427%, and 0.136% of the total body weight increment, respectively. Considering fat accumulation in the abdomen and around internal organs in mice, we extrapolated that the body weight increase was largely related to a fat content increase. In addition, serum TC, LDL-C, HDL-C, and glucose levels had a marked elevation after high-fat feeding ($p<0.01$, Fig. 1F–J). Serum ALT and AST levels in HFD-fed mice showed increasing trends than those in ND-fed mice (ALT, 147.40 ± 47.61 U/L vs 43.17 ± 2.67 U/L, $p = 0.32$; AST, 374.80 ± 101.80 U/L vs 189.90 ± 15.16 U/L, $p = 0.41$). Taken together, male C57BL/6J mice fed HFD for 24 weeks developed obesity and hyperlipidemia.

doi: 10.3164/jcbn.22-73

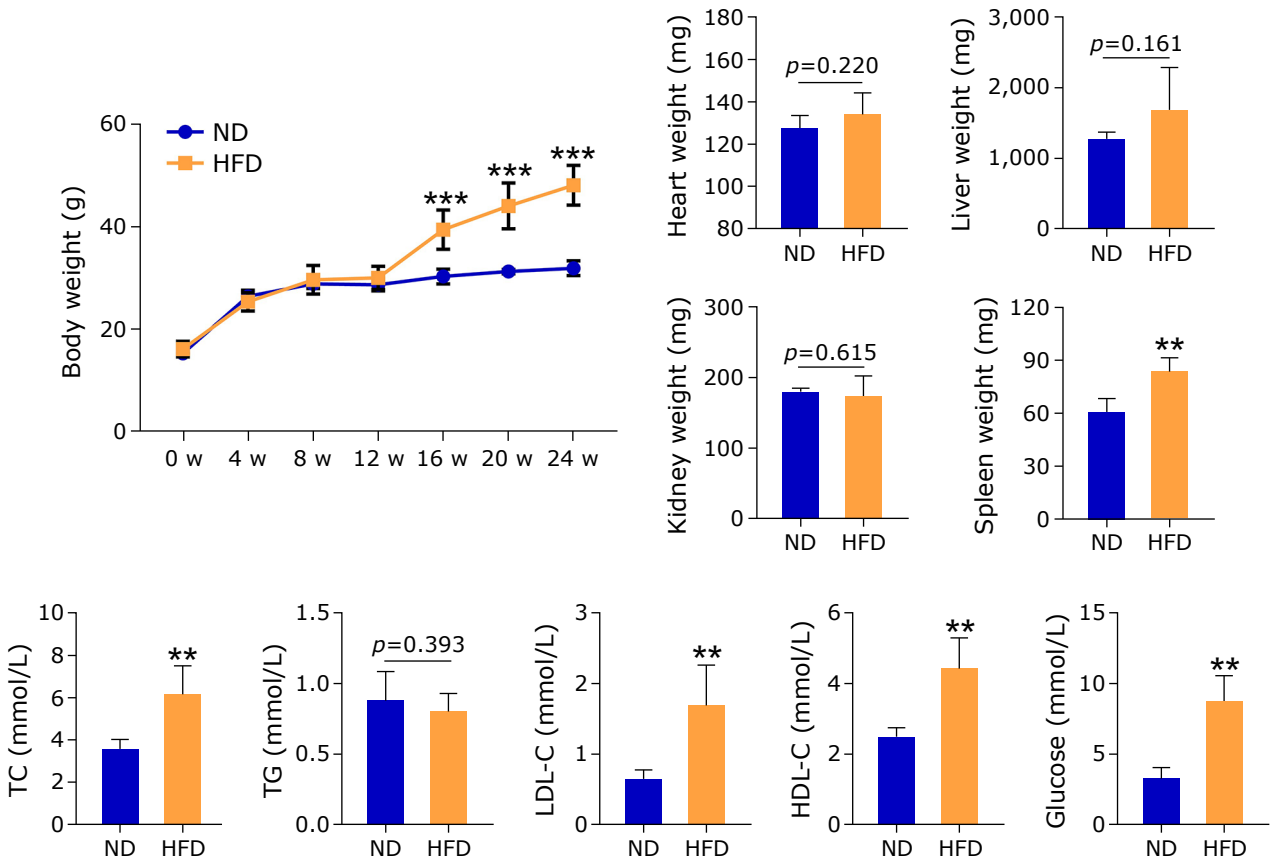

Fig. 1. High-fat diet feeding induced body weight gain and hyperlipidemia in C57BL/6J male mice. (A) Body weight changes at 0–24 weeks of feeding. (B–E) Heart, liver, kidney, and spleen weights. (F–J) TC, TG, LDL-C, HDL-C, and glucose levels. Data are presented as mean ± SD. Normal diet (ND, $n = 5$); High-fat diet (HFD, $n = 9$). $^{**}p<0.01$ or $^{***}p<0.001$ vs ND group. See color figure in the on-line version.

High-fat feeding resulted in pathological tissue changes in multiple organs of mice. In the present study, compared with ND-fed mice, the hearts of HFD-fed mice presented increased cardiomyocyte size ($p<0.01$), disorganized myofiber, aggravated interstitial fibrosis (Masson's staining, $p<0.01$), and reduced vessel density (α-SMA, $p<0.01$) (Fig. 2A–E). Contrary to cardiac muscle, the histology and collagen content of the skeletal muscle didn't change obviously after high-fat consumption (Fig. 2F and H). HFD feeding resulted in higher arterial wall thickness and intimal-medial thickness in the thoracic aorta of mice ($p<0.05$, Fig. 2G, J, and K). The elastin within the wall of the thoracic aorta of HFD-fed mice was disorganized in most regions (Fig. 2G). Moreover, HFD-fed mice showed widened alveolar septum, infiltrated inflammatory cells, and increased collagen accumulation in the alveolar septum ($p<0.01$) and peribronchial regions ($p<0.01$) of the lung (Fig. 3A and B). High-fat feeding resulted in hepatic steatosis, characterized by swollen hepatocytes and narrowed space between liver plates (Fig. 3C and D). The structural changes occurred in the kidneys of HFD-fed mice, including tubular dilatation and swelling, local tubular cell vacuolization, inflammatory cell infiltration, capsular space expansion, and glomerular retraction (Fig. 3E). The kidney injury score of HFD-fed mice was higher than that in ND-fed mice ($p<0.05$, Fig. 3F). Furthermore, high-fat consumption resulted in significant splenomegaly, an expansive red pulp area, a decreased white pulp region, increased splenic macrophages adjacent to the sinusoids ($p<0.05$), and lipid deposition in the spleen of mice (Fig. 3G and H).

Glycogen content was increased in the liver and skeletal muscle of HFD-fed mice. In adult cardiomyocytes, the glycogen content occupies about 2% of the cell volume.[13] High-fat consumption did not affect the glycogen contents (PAS staining) in the hearts ($p = 0.29$, Fig. 2A and D), kidneys ($p = 0.82$, Fig. 3E and F), or spleens ($p = 0.0508$, Fig. 3G and H). Normally, glycogen is stored in the skeletal muscles as an energy reserve to supply glucose to the muscle cells during contraction. The liver is another glycogen-storage tissue.[14] Significant elevations of glycogen in the skeletal muscles ($p<0.05$, Fig. 2F and I) and liver ($p<0.0001$, Fig. 3C and D) of HFD-fed mice, accompanied by increased blood glucose levels, were observed in this study.

HFD feeding resulted in mitochondrial ultrastructural impairments in multiple organs. The abundant and orderly organized mitochondria with few heteromorphic changes were found in the hearts of ND-fed mice, while the most mitochondria in the hearts of HFD-fed mice showed heteromorphic changes with disorganization, swollen, vacuolization, and decreased electron dense structures (Fig. 4A). High-fat feeding increased the number of mitochondria in the skeletal muscles of mice in this study, which is consistent with the previous reports.[15,16] A part of the mitochondria in the skeletal muscles of HFD-fed mice showed irregular shape, swelling, and local vacuolization (Fig. 4B). The proportions of defective mitochondria in the hearts and skeletal muscles of HFD-fed mice were significantly higher than those of ND-fed mice (Fig. 4C). Additionally, the number of lipid droplets (LDs; red arrow, Fig. 4A and B) in the hearts and skeletal muscles of HFD-fed mice was increased, and some of

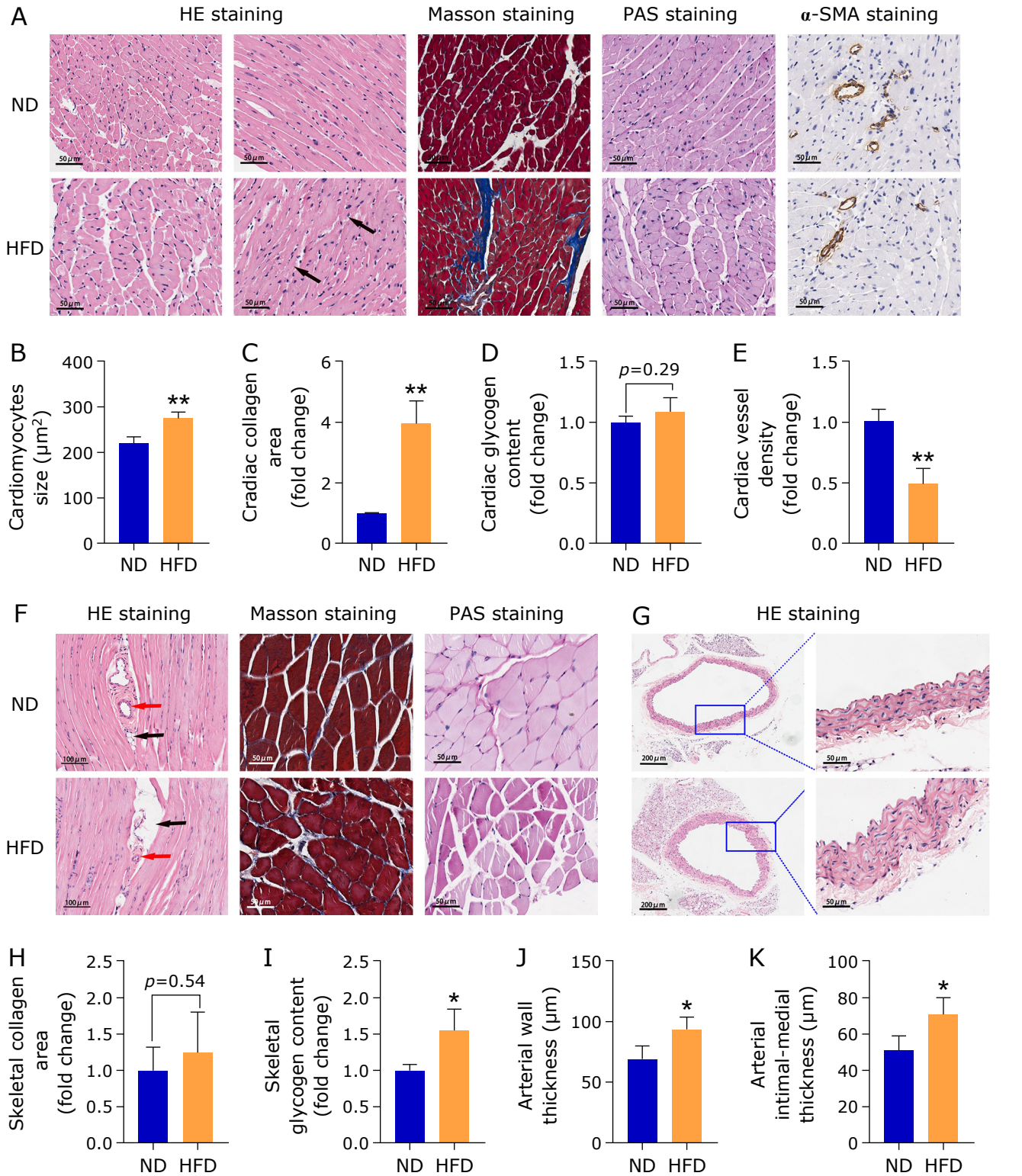

Fig. 2. Histopathological changes of the heart, skeletal muscle, and thoracic aorta of HFD-fed mice. (A) Representative images of HE, Masson's, PAS staining, and α-SMA immunochemistry of the heart. Disorganized myocardium (black arrow). (B–E) (Semi-) Quantitative analysis of cardiomyocyte size, cardiac collagen area, glycogen content, and α-SMA expression ($n = 3$). (F) Representative images of HE, Masson's, and PAS staining of skeletal muscle. Vessels (red arrow), fat deposition (black arrow). (G) Representative images of HE staining of the thoracic aorta. (H, I) (Semi-) Quantitative analysis of skeletal collagen area and glycogen content ($n = 3$). (J, K) Quantitative analysis of arterial wall thickness and intimal-medial thickness of the thoracic aorta ($n = 3$). Data are presented as mean ± SD. Normal diet (ND) or high-fat diet (HFD). The cardiomyocyte size was obtained by averaging the data of 30 to 45 cardiomyocytes from three different regions of the left ventricle per section from 3 per group using ImageJ software. Four to six high-resolution fields per section from 3 in each group were randomly selected to perform (semi-) quantitative analysis by IPP 6.0. *p<0.05 or **p<0.01 vs ND group. See color figure in the on-line version.

doi: 10.3164/jcbn.22-73

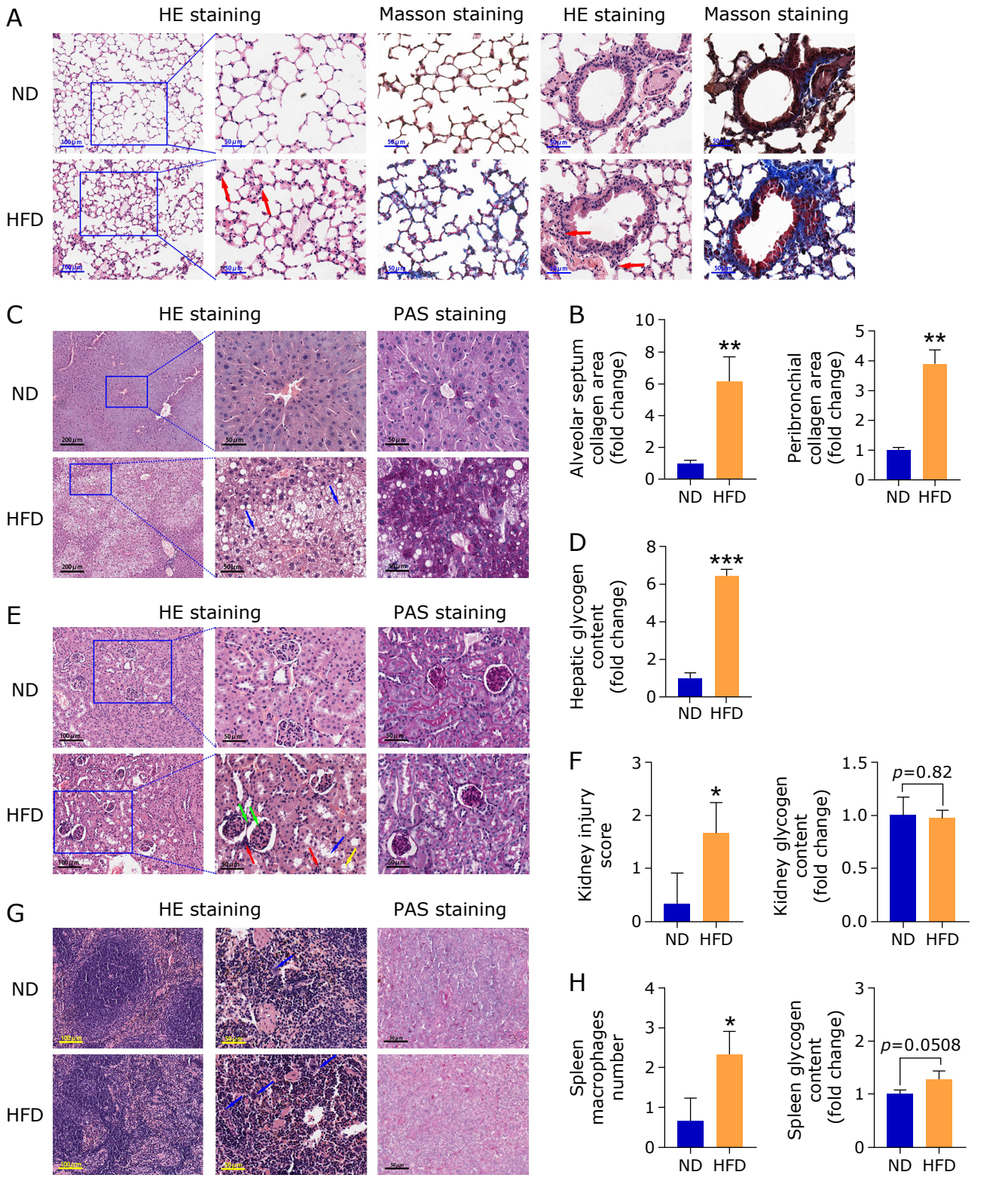

Fig. 3. Histopathological changes of the lung, liver, kidney, and spleen of mice. (A) Representative images of HE and Masson's staining of the lung. Infiltrated inflammatory cells (red arrow). (B) Semi-quantitative analysis of alveolar septum and peri-bronchial collagen content ($n = 3$). (C) Representative images of HE and PAS staining of the liver. Swollen hepatocytes (blue arrow). (D) Semi-quantitative analysis of hepatic glycogen content ($n = 3$). (E) Representative images of HE and PAS staining of the kidney. Tubular dilatation (blue arrow), infiltrated inflammatory cells (red arrow), vacuolized tubular (yellow arrow), augmented capsular space, and shrunken glomeruli (green arrow). (F) Semi-quantitative analysis of kidney injury score and glycogen content ($n = 3$). (G) Representative images of HE and PAS staining of the spleen. Spleen macrophages (blue arrow). (H) (Semi-) Quantitative analysis of spleen macrophages number and glycogen content ($n = 3$). Data are presented as mean ± SD. Normal diet (ND) or high-fat diet (HFD). Four to six high-resolution fields per section from 3 mice in each group were randomly selected to perform (semi-) quantitative analysis by IPP 6.0. *p<0.05, **p<0.01 or ***p<0.001 vs ND group. See color figure in the on-line version.

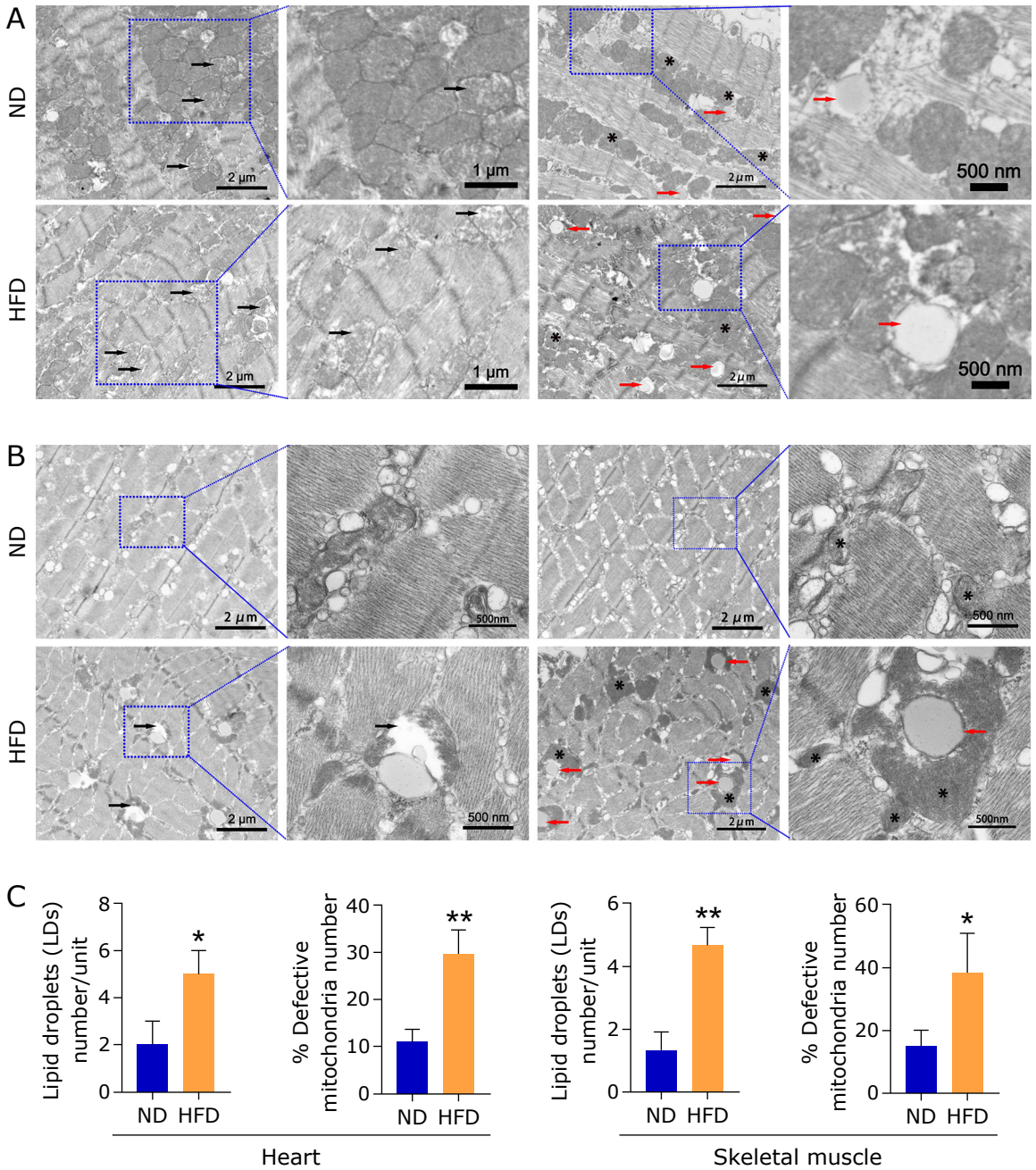

Fig. 4. Ultrastructure of the heart and skeletal muscle of mice. (A) Representative transmission electron microscope (TEM) images of the heart. (B) Representative TEM images of the skeletal muscle. Mitochondria (*), lipid droplets (LDs, red arrow), impaired mitochondria (black arrow). (C) Quantitative analysis of the numbers of lipid droplet per unit and the percentage of defective mitochondria ($n = 3$, each group). Data are presented as mean ± SD. Normal diet (ND) or high-fat diet (HFD). *p<0.05, or **p<0.01 vs ND group. See color figure in the on-line version.

LDs were inserted into the mitochondria (Fig. 4A–C).

In this study, the basal compartment of proximal tubular epithelial cells (PTECs) in ND-fed mice was rich in parallelly distributed mitochondria, which enabled active transport processes with Na^+-K^+-ATPase. On the contrary, small and a few mitochondria were disarrayed in the same position as in HFD-fed mice (Fig. 5A). A part of the mitochondria in the PTECs of HFD-fed mice exhibited shorter and rounder shapes and heteromorphic changes, characterized by swollen, vacuolization, and decreased electron dense structures. The proportion of defective mitochondria and the number of LDs in the PTECs of HFD-fed mice were significantly higher than those of ND-fed mice (Fig. 5A and C). Additionally, podocytes and glomerular basement membrane presented intoxicated appearances, including foot process fusion or effacement, slit diaphragm narrowing, and local glomerular basement membrane thickening in the kidneys of HFD-fed mice (Fig. 5A).

In the livers of HFD-fed mice, mitochondria were obscured with local swelling, and the endoplasmic reticulum (ER) was destructed, accompanied by ribosomal degranulation (double red arrow, Fig. 5B). Furthermore, the proportions of defective mitochondria in the livers of HFD-fed mice were significantly higher than those of ND-fed mice. The number of autophagosomes or autophagy lysosomes (labeled by green arrow, Fig. 5B) in the

doi: 10.3164/jcbn.22-73

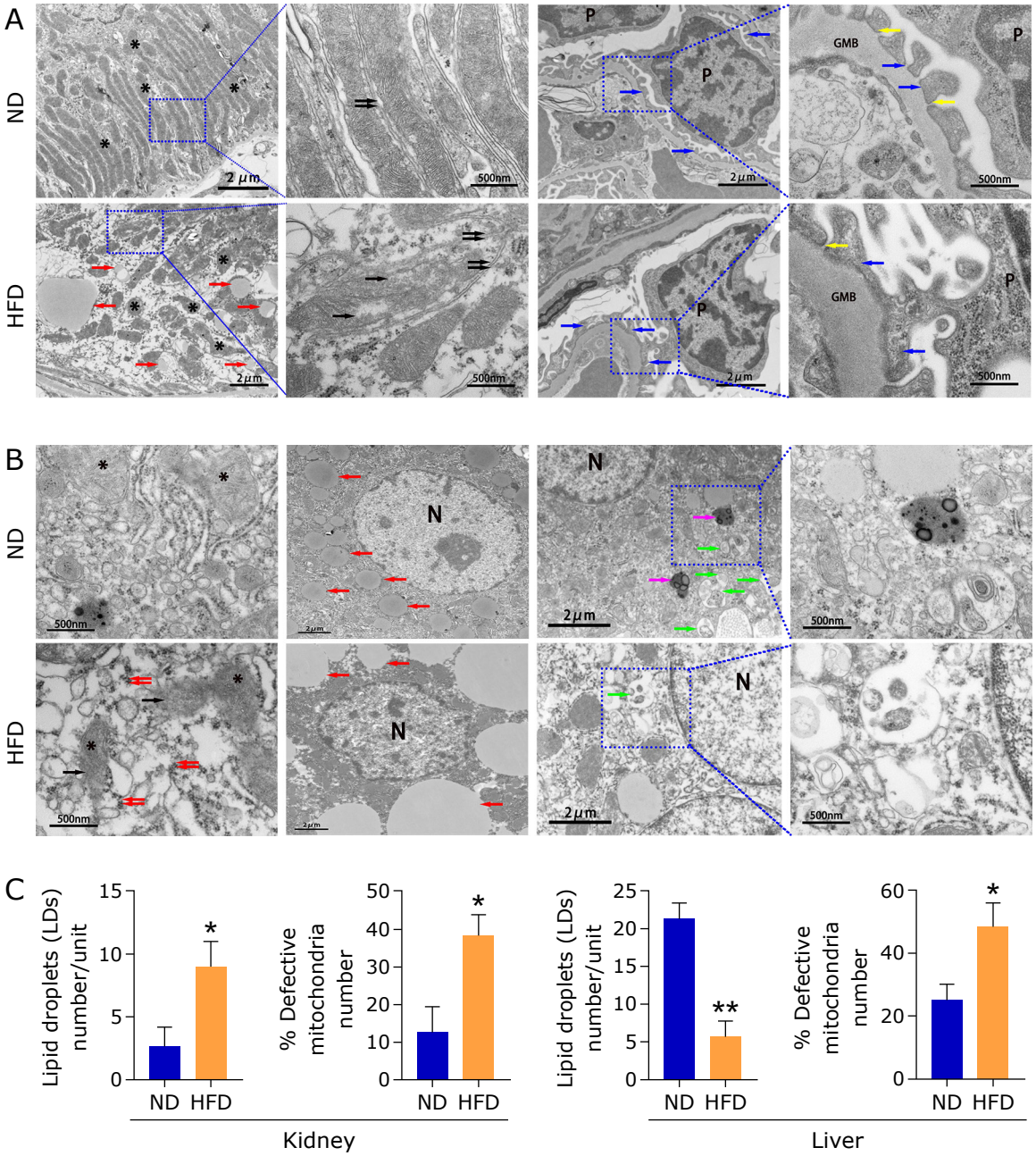

Fig. 5. Ultrastructure of the kidney and liver of mice. (A) Representative transmission electron microscope (TEM) images of the kidney. (B) Representative TEM images of the liver. (C) Quantitative analysis of the numbers of lipid droplet per unit and the percentage of defective mitochondria ($n = 3$, each group). Mitochondria (*), lipid droplets (LDs, red arrow), impaired mitochondria (black arrow), enfolded plasma membrane (double black arrow), podocyte (P), foot process (blue arrow), glomerular basement membrane (GMB), filtration pore (yellow arrow), nucleus (N), ribosomal degranulation (double red arrow), autophagosome or autophagy lysosomes (green arrow), telolysosome (magenta arrow), Data are presented as mean ± SD. Normal diet (ND) or high-fat diet (HFD). *p<0.05, or **p<0.01 vs ND group. See color figure in the on-line version.

livers of HFD-fed mice was less than that of ND-fed mice, suggesting that autophagy may be inhibited in the livers by high-fat feeding. Additionally, in the hepatocytes of HFD-fed mice, the nucleus size was decreased, accompanied by a reduced number and an enlarged size of LDs compared to ND-fed mice (Fig. 5B and C).

HFD feeding led to elevated cellular apoptosis levels in heart, liver, and kidney. Given that mitochondrial dysfunction participates in the intrinsic cellular apoptosis pathway, and increased apoptosis reflects the disruption of organismal homeostasis maintenance,[15] we next examined the apoptosis levels in multiple organs by TUNEL analysis. High-fat consumption resulted in elevated apoptosis in the hearts (p<0.05), livers (p<0.01), and kidneys (p<0.05) (Fig. 6A and B), but not in the skeletal muscles (p>0.05).

HFD feeding led to imbalanced expression of proteins related to mitochondrial dynamics in multiple organs. Given the important roles of mitochondrial fusion/fission and biogenesis/degradation in regulating the mitochondrial form, size, and function, we examined the mitochondrial dynamics protein expression in multiple organs. As shown in Fig. 7A–D, high-fat consumption decreased TFAM (biogenesis) expression,

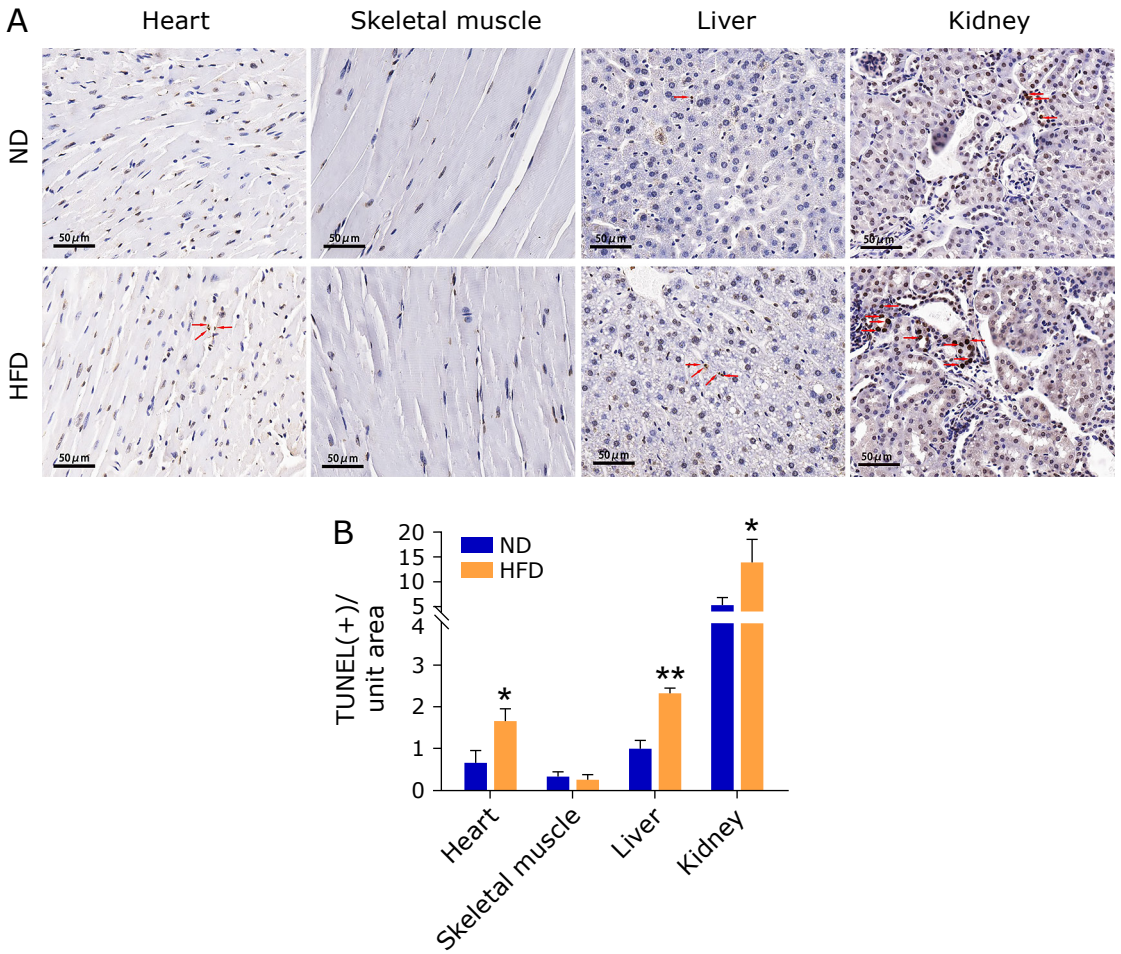

Fig. 6. Assessment of cellular apoptosis levels in the heart, skeletal muscle, liver, and kidney of mice. (A) Representative apoptosis images of the heart, skeletal muscle, liver, and kidney. Apoptosis cell (red arrow). (B) Quantitative analysis of cellular apoptosis levels in heart, skeletal muscle, liver, and kidney ($n = 3$). Data are presented as mean ± SD. Normal diet (ND) or high-fat diet (HFD). Positive cells were counted from 4 to 6 fields per section from 3–4 mice in each group. *p<0.05 or **p<0.01 vs ND group. See color figure in the on-line version.

increased LC3 (autophagy) expression, and simultaneously downregulated PINK1 (mitophagy), DRP1 (fission), MFN2 (fusion), and OPA1 (fusion) expression in the hearts of mice (p<0.05). Cytosolic LC3-I is conjugated to phosphatidylethanolamine to become LC3-II, which is reliably associated with the formation of autophagosomes.[16] Therefore, we calculated the ratio of LC3-II to LC3-I to detect LC3 conversion. The LC3-II: LC3-I ratio and the MFN1 (fusion) expression were not changed in the myocardium by high-fat feeding. The changes in mitochondrial dynamics proteins in the skeletal muscles of HFD-fed mice were different from those in the hearts (Fig. 8). The TFAM expression was enhanced (p<0.05), while the expression of LC3 and PINK1 and the ratio of LC3-II to LC3-I were not changed in the skeletal muscles of HFD-fed mice. The enhanced mitochondrial biogenesis (TFAM) was consistent with the mitochondrial content increment in the skeletal muscles of HFD-fed mice. DRP1 expression was increased, while MFN2 and OPA1 expression were decreased in the skeletal muscles of HFD-fed mice (Fig. 8).

High-fat feeding resulted in the upregulated expression of DRP1 and the downregulated expression of MFN2, OPA1, and TFAM in the kidneys (p<0.05, Fig. 9C and D). It was noted that the expression alterations in DRP1 and MFN2 mainly occurred in the tubular epithelial cells of HFD-fed mice (Fig. 9A and B). DRP1, MFN2, and OPA1 expression were significantly downregulated (p<0.05), while LC3 and TFAM expression were upregulated in the livers of HFD-fed mice (Fig. 9E and F). LC3 expression was significantly upregulated (p<0.05), while the ratio of LC3-II to LC3-I and the expression of TFAM, MFN2, and OPA1 were downregulated in the spleens of HFD-fed mice (Fig. 10).

Taken together, the expression of TFAM was increased in the skeletal muscles and livers, decreased in the hearts, kidneys, and spleens of HFD-fed mice. The expression of LC3 was increased in the hearts, livers, and spleens of HFD-fed mice, and unchanged in the skeletal muscles and kidneys of HFD-fed mice. However, the ratio of LC3-II to LC3-I was decreased only in the spleens of HFD-fed mice and unchanged in other tissues of HFD-fed mice. The expression of PINK1 was only altered in the hearts of HFD-fed mice. The expression of DRP1 was increased in the skeletal muscles and kidneys, decreased in the hearts and livers, and unchanged in the spleens of HFD-fed mice. The significantly downregulated MFN2 and OPA1 proteins were the shared alterations in the hearts, kidneys, livers, spleens, and skeletal muscles of HFD-fed mice. The expression of MFN1 in these organs was unchanged.

HFD feeding led to alteration of OXPHOS and mitochondrial outer membrane protein expression in multiple organs. Furthermore, we examined the expression of mitochondrial outer membrane and OXPHOS protein (TOMM20 and

doi: 10.3164/jcbn.22-73

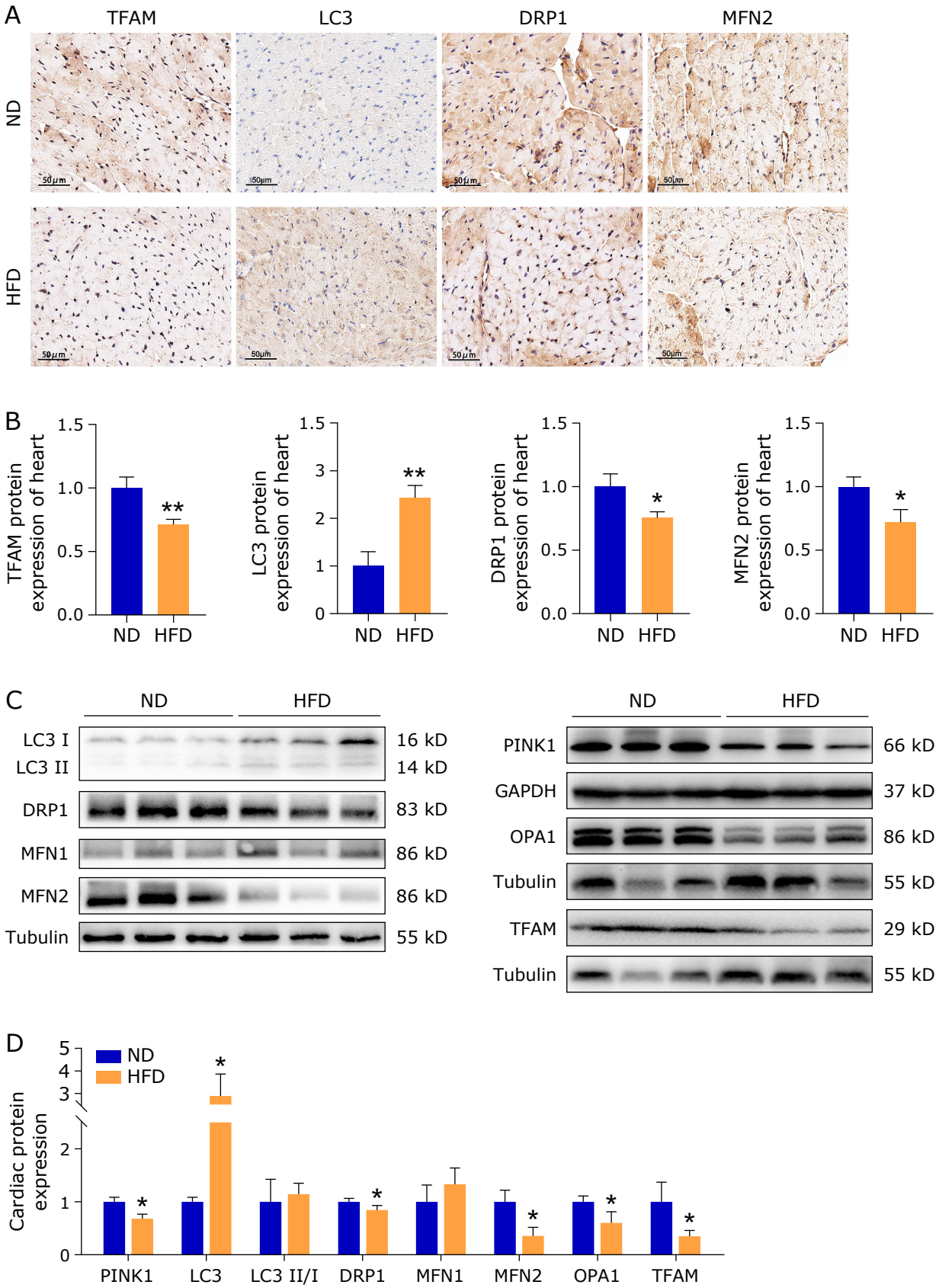

Fig. 7. Assessment of mitochondrial dynamics protein expression in the heart of mice. (A, B) Representative immunohistochemistry images and relative quantification of TFAM, LC3, DRP1 and MFN2 expression in the heart of mice. (C, D) Western blot analysis and semi-quantification of LC3-I, LC3-II, DRP1, MFN1, MFN2, PINK1, OPA1, and TFAM expression in the heart of mice. Tubulin or GAPDH is used as internal control in Western blot analysis. Data are presented as mean ± SD ($n = 3$). Normal diet (ND) or high-fat diet (HFD). Four to six high-resolution fields per section of immunohistochemistry results from 3 mice in each group were randomly selected to be analyzed by IPP 6.0. *p<0.05 or **p<0.01 vs ND group. See color figure in the on-line version.

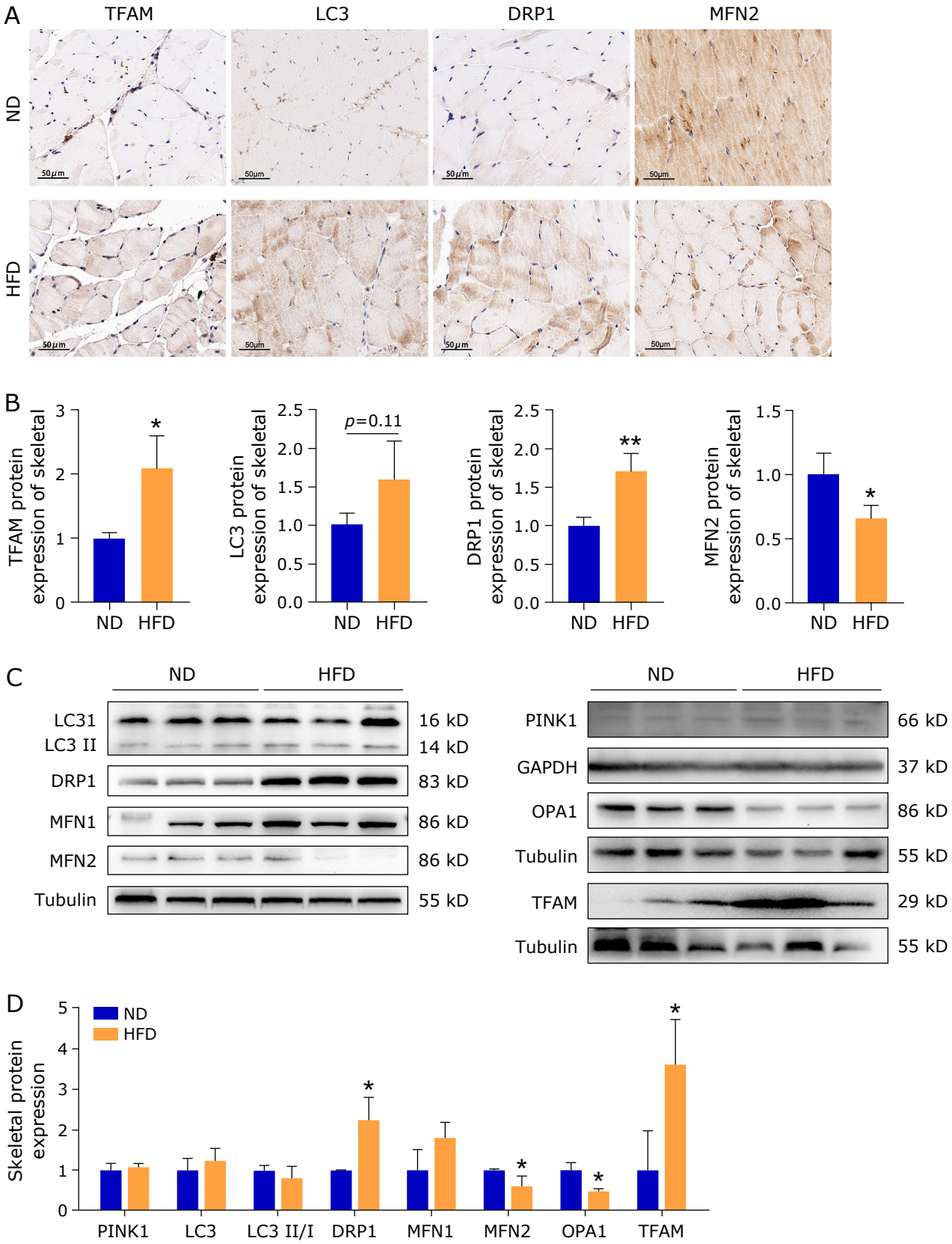

Fig. 8. Assessment of mitochondrial dynamics protein expression in the skeletal muscle of mice. (A, B) Representative immunohistochemistry images and relative quantification of TFAM, LC3, DRP1, and MFN2 expression in the skeletal muscle of mice. (C, D) Western blot analysis and semi-quantification of LC3-I, LC3-II, DRP1, MFN1, MFN2, PINK1, OPA1, and TFAM expression in the skeletal muscle of mice. Tubulin or GAPDH is used as internal control in Western blot analysis. Data are presented as mean ± SD ($n = 3$). Normal diet (ND) or high-fat diet (HFD). Four to six high-resolution fields per section of immunohistochemistry results from 3 mice in each group were randomly selected to be analyzed by IPP 6.0. *$p<0.05$ or **$p<0.01$ vs ND group. See color figure in the on-line version.

doi: 10.3164/jcbn.22-73

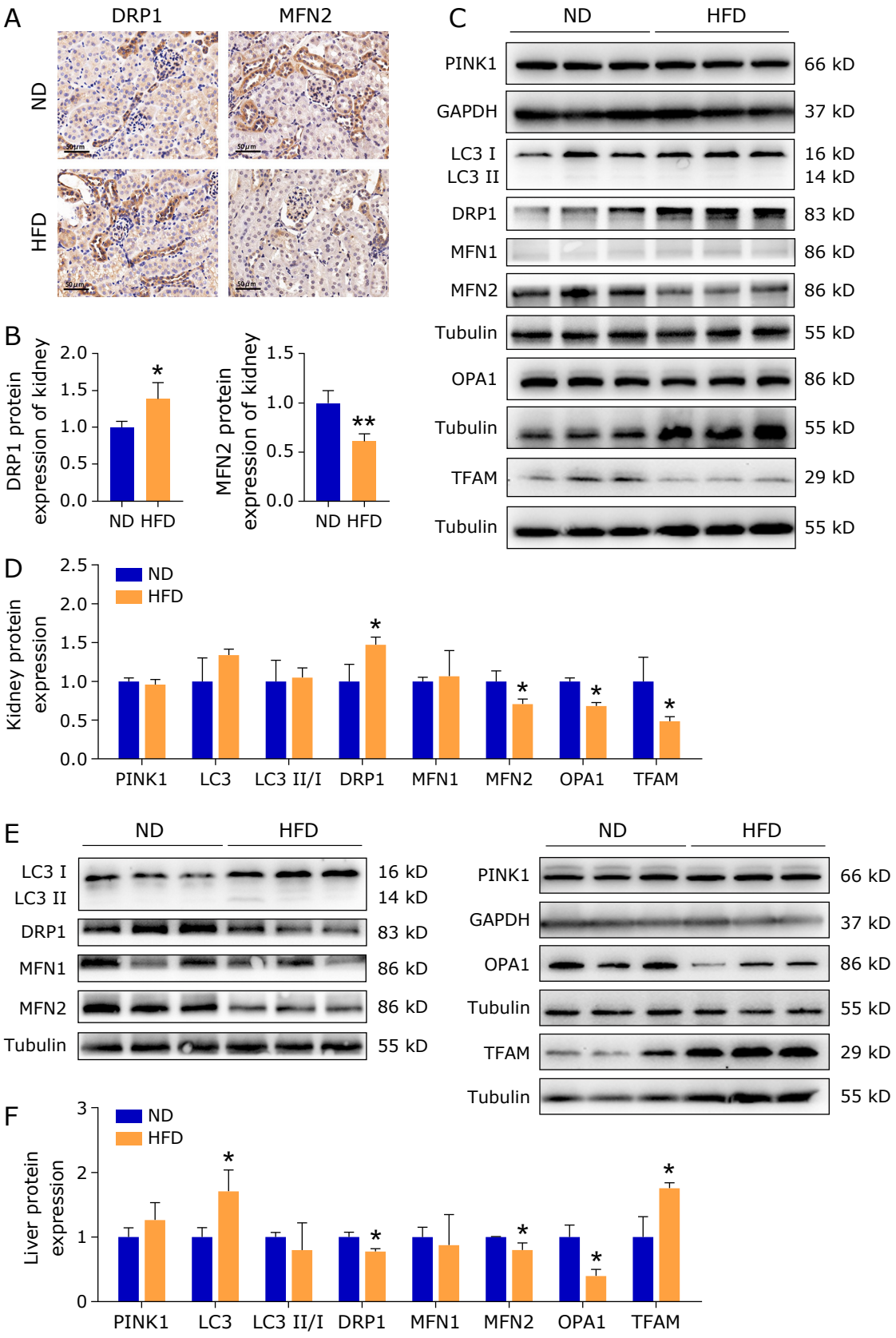

Fig. 9. Assessment of mitochondrial dynamics proteins expression in the kidney and liver of mice. (A, B) Representative immunohistochemistry images and relative quantification of DRP1 and MFN2in the kidney of mice. (C, D) Western blot analysis and semi-quantification of LC3-I, LC3-II, DRP1, MFN1, MFN2, PINK1, OPA1, and TFAM expression in the kidney of mice. (E, F) Western blot analysis and semi-quantification of LC3-I, LC3-II, DRP1, MFN1, MFN2, PINK1, OPA1, and TFAM expression in the liver of mice. Tubulin or GAPDH is used as internal control in Western blot analysis. Data are presented as mean ± SD ($n = 3$). Normal diet (ND) or high-fat diet (HFD). Four to six high-resolution fields per section of immunohistochemistry result from 3 in mice each group were randomly selected to be analyzed by IPP 6.0. *p<0.05 or **p<0.01 vs ND group. See color figure in the on-line version.

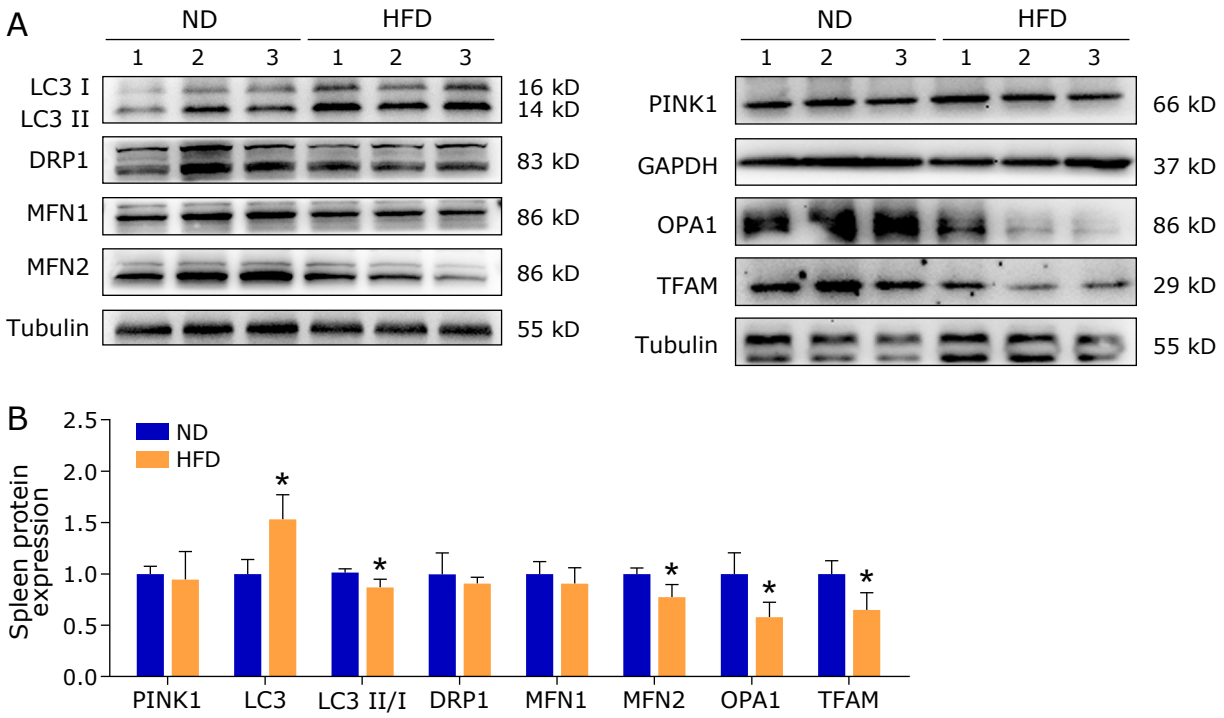

Fig. 10. Assessment of mitochondrial dynamics proteins expression in the spleen of mice. (A, B) Western blot analysis and semi-quantification of LC3-I, LC3-II, DRP1, MFN1, MFN2, PINK1, OPA1, and TFAM expression in the spleen of mice. Tubulin or GAPDH is used as internal control in Western blot analysis. Data are presented as mean ± SD (n = 3). Normal diet (ND) or high-fat diet (HFD). *p<0.05 vs ND group. See color figure in the on-line version.

ATP5A) in multiple organs (Fig. 11). ATP5A is a catalytic subunit of the mitochondrial ATP synthase (complex V) responsible for the synthesis/hydrolysis of ATP.[17] TOMM20 is the receptor subunit of the mitochondrial membrane import pore, which allows the import of nuclear encoded OXPHOS subunits and induces OXPHOS.[18] TOMM20 and ATP5A are located at the outer and inner mitochondrial membrane and have been used as markers of mitochondrial mass and metabolic activity. In this study, TOMM20 protein was significantly increased in the hearts, skeletal muscles, and spleens (p<0.05), decreased in the kidneys (p<0.05), and unchanged in the livers of HFD-fed mice. The ATP5A protein was increased in the hearts and skeletal muscles (p<0.05), and unchanged in the kidneys, livers, and spleens of HFD-fed mice.

Discussion

In this study, we systemically evaluated the pathological tissue changes, mitochondrial structure, and mitochondrial dynamics protein expression in multiple organs of HFD-fed mice. The association between high-fat consumption and systemic chronic illness is raising concerns in the clinic. Obesity and hyperlipidemia, which are positively associated with dietary fat intake, are considered as risk factors for many chronic diseases.[19–22] In the present study, we confirmed the existence of multiple organs remodeling after high-fat consumption, including the heart, aorta, kidney, lung, and liver. The overall impact of high-fat consumption on organ remodeling is multifactorial and still needs to be investigated. HFD-induced chronic systemic low-grade inflammation and oxidative stress are reported to be the underlying mechanisms.[23–25]

Mitochondria play a central role in the biology of most eukaryotic cells, because mitochondria are involved in catabolic and anabolic metabolism, regulation of intracellular calcium homeostasis, initiation of inflammatory reactions, and control of multiple pathways determined cell death. The mitochondrial impairment has been demonstrated to be tightly linked to progressive organ remodeling or organ failure.[4,7,26,27] In this study, we confirmed that the mitochondrial change is a shared phenomenon for various organ remodeling in HFD-fed mice, especially the tissues or cells with high energy demands from mitochondrial OXPHOS, such as cardiomyocytes and PTECs. Mitochondria occupy approximately 35–40% cytoplasmic volume in cardiomyocytes and provide 90% ATP energy during OXPHOS to match high energy demands of heart.[28] In kidney, proximal tubular reabsorption allows for 65–75% of all tubular reabsorption to water and sodium, and 90% to proteins and glucose. Hence, PTECs are highly energy-demanding and rich in mitochondria. PTECs injury leads to renal reabsorption dysfunction.[29] Therefore, cardiomyocytes and PTECs are more sensitive to lipid toxicity, and lipid-attributed mitochondrial damage is particularly catastrophic for cardiomyocytes and PTECs.[29]

Healthy mitochondria maintain their stability through balancing two opposed processes: mitochondrial fission/fusion and mitochondrial biogenesis/degradation (including mitophagy). LC3 (LC3-II:LC3-I ratio) and PINK1 are the markers of autophagy and mitophagy, respectively. TFAM is required in mitochondrial biogenesis. DRP1 is the cytosol-located GTPase that mediated the mitochondrial fission process. MFN1/2 and OPA1 are mitochondrial membrane-located GTPases which control the mitochondrial outer and inner mitochondrial membrane fusion, respectively.[30,31] MFN1 and MFN2 belong to the family of ubiquitous transmembrane GTPases, which share approximately 80% similarity and the same relevant structural motifs.[32] MFN1 has higher GTPase activity than MFN2. MFN2, but not MFN1, possesses a proline-rich region, which is involved in protein-protein interactions.[32] In this study, we proved that the impact of HFD on mitochondrial biogenesis (TFAM), autophagy or mitophagy (LC3 or PINK1), and fission (DRP1) appeared to be tissue-specific. On the contrary, the impact of HFD on mito-

doi: 10.3164/jcbn.22-73

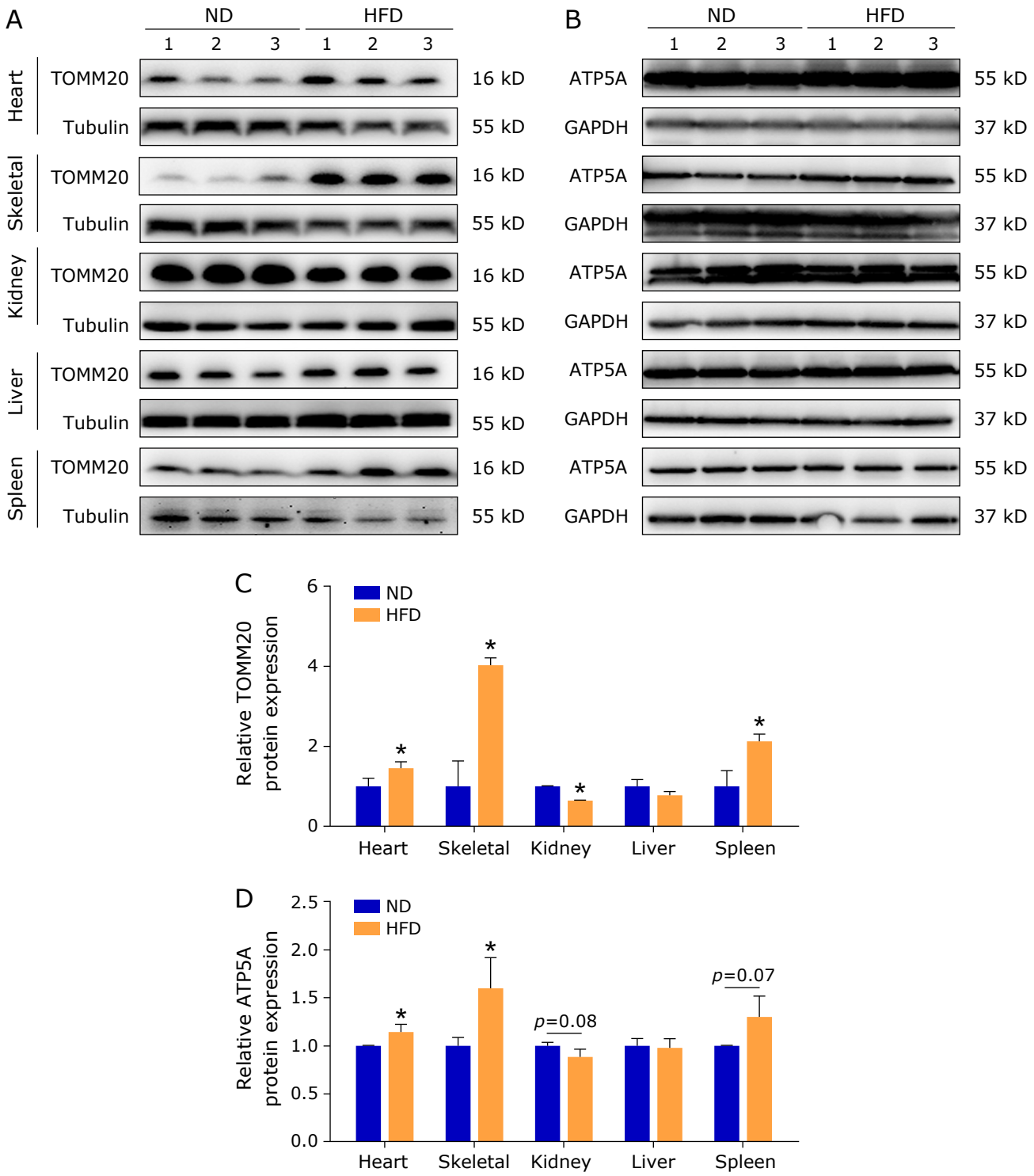

Fig. 11. Assessment of mitochondrial markers TOMM20 and ATP5A expressions in multiple organs of mice. (A) Western blot analysis of TOMM20. Tubulin is used as an internal control. (B) Western blot analysis of ATP5A. GAPDH is used as an internal control. (C) Semi-quantification of TOMM20 expression. (D) Semi-quantification of ATP5A expression. Data are presented as mean ± SD (n = 3). Normal diet (ND) or high-fat diet (HFD). *p<0.05 vs ND group. See color figure in the on-line version.

chondrial fusion (MFN2 and OPA1) was consistent in different tissues. The significantly downregulated expressions of MFN2 and OPA1, but not MFN1, were the shared alterations in the heart, kidney, liver, spleen, and skeletal muscle of HFD-fed mice. The results are consistent with most previous studies on mitochondrial fusion protein changes in the obesity or metabolic disease, which proved that MFN2 and/or OPA1 were significantly reduced in the tissue or cell of skeletal muscle,[33–39] fat,[40,41] hypothalamus,[42] kidney,[43] heart,[44–47] liver,[48] etc. On the contrary, a few studies reported that MFN2 was increased in

the heart and liver,[49,50] unchanged in the fat,[50] skeletal muscle or cell of metabolic disease.[51,52] In addition, some studies proved the reduction of MFN1 in the heart and liver of animal with metabolic disease.[44,53,54] In this study, we confirmed that the high-fat consuming caused the decreasing of mitochondrial fusion proteins MFN2 and OPA1 in the heart, skeletal muscle, kidney, and liver, which are high-energy-demanding or metabolic-related organs. Meanwhile, the spleen, the organ of the lymphatic system, also presented mitochondrial fusion proteins MFN2 and OPA1 downregulation after HFD feeding. This is reported for the first time. The mitochondrial change in the spleen of metabolic disease is not as well-known as other organs.[55] The mitochondrial quality control in the spleen of metabolic disease needs to be further investigated.

The balance between nutrient demand and supply is associated with mitochondrial fission and fusion balance. Previous researches prove that metabolic oversupply is followed by fragmentation of mitochondria (enhanced fission), which leads to a decrease in mitochondrial bioenergetic efficiency that, in association with an increase in nutrient storage, will avoid energy waste. Whereas, metabolic undersupply results in elongated mitochondria (enhanced fusion) to increase mitochondrial bioenergetic efficiency and sustain the energy need.[32] HFD provides a rich nutrient environment. Our research and the previous studies confirmed that the downregulation of MFN2 and OPA1 in multiple organs led to a weakening of the fusion process. The disruption of the balance between mitochondrial fission and fusion resulted in enhanced fission with fragmentation of mitochondria. The repression of MFN2 is not just limited to the dysregulation of mitochondrial shape. The mitochondrial dysfunctions, such as glucose oxidation reduction, mitochondrial membrane potential depolarization, and mitochondrial proton leak are also caused by MFN2 repression.[38,56] MFN2 deficiency in the skeletal muscle induced by obesity was associated with a decrease in the subunits of complexes I, II, III, and V.[57] MFN2 activates mitochondrial energization, partly by regulating OXPHOS expression through the role independent of mitochondrial fusion protein.[57] Moreover, the MFN2 protein has extramitochondrial roles. For example, MFN2 forms an endoplasmic reticulum (ER)-mitochondria contact site, which is important for cell proliferation, autophagy, calcium signaling, inflammation, and so on.[30] The OPA1 protein is necessary for mitochondrial inner membrane fusion.[58] Moreover, OPA1 contributes to mitochondrial cristae morphology, maintains mtDNA integrity and copy number, regulates apoptotic cristae remodeling, and stabilizes respiratory chain.[58,59] OPA1 facilitates cell-autonomous adipocyte browning and involves in lipogenesis and triglyceride synthesis pathways.[41,60] The treatments for metabolic disease, such as exercise, could reverse the down-expression of MFN2 and OPA1.[61,62] On the other hand, the MFN2 overexpression could recover impaired insulin sensitivity induced by HFD feeding.[63] The mitochondrial fusion proteins may become promising therapeutic targets and/or markers for metabolic disease.[30,64] In this study, the reduction of mitochondrial fusion did not cause the synchronous change of mitochondrial OXPHOS function, indicating its strong compensatory effect.

This study includes several limitations. The key regulators of MFN2 and OPA1, such as transcription factor estrogen-related receptor-alpha, peroxisome proliferator-activated receptor gamma coactivator (PGC)-1α and PGC-1β,[65] and the mitochondrial proteases (such as OMA1, which mediates proteolysis of OPA1) were not detected.[66] In addition, we can't obtain clear TEM image of cristae morphology due to some technical problems. Therefore, whether the cristae morphology disruption correlated with OPA1 downregulation will be proved in future study.

Conclusion

The results of our study indicated that high-fat feeding led to pathological tissue changes in multiple organs, accompanied by mitochondrial ultrastructural damage, MFN2 and OPA1 downregulation. Developing the agents targeting mitochondrial protection for clinical therapy of obesity-attributed complications might be a potential strategy in the future.

Author Contributions

All authors have contributed significantly to this work. Conceptualization: PZ, DY, and XC; Methodology: PZ and WM; Formal analysis and investigation: PZ, WM, NL, YG, ZB, DY, HW, and XC; Data curation: PZ, WM, YG, and ZB; Visualization: PZ and XC; Writing – original draft preparation: PZ; Writing – review and editing: DY and XC; Funding acquisition: DY.

Data Availability Statement

All data generated or analyzed during this study are available from the corresponding authors on reasonable request.

Conflict of Interest

No potential conflicts of interest were disclosed.

References

1 Hariri N, Thibault L. High-fat diet-induced obesity in animal models. *Nutr Res Rev* 2010; **23**: 270–299.
2 Fava MC, Agius R, Fava S. Obesity and cardio-metabolic health. *Br J Hosp Med (Lond)* 2019; **80**: 466–471.
3 GBDO 2015 Collaborators, Afshin A, Forouzanfar MH, *et al*. Health effects of overweight and obesity in 195 countries over 25 years. *N Engl J Med* 2017; **377**: 13–27.
4 Bonora M, Wieckowski MR, Sinclair DA, Kroemer G, Pinton P, Galluzzi L. Targeting mitochondria for cardiovascular disorders: therapeutic potential and obstacles. *Nat Rev Cardiol* 2019; **16**: 33–55.
5 Ni HM, Williams JA, Ding WX. Mitochondrial dynamics and mitochondrial quality control. *Redox Biol* 2015; **4**: 6–13.
6 Meyer JN, Leuthner TC, Luz AL. Mitochondrial fusion, fission, and mitochondrial toxicity. *Toxicology* 2017; **391**: 42–53.
7 Nunnari J, Suomalainen A. Mitochondria: in sickness and in health. *Cell* 2012; **148**: 1145–1159.
8 Heyne E, Schrepper A, Doenst T, Schenkl C, Kreuzer K, Schwarzer M. High-fat diet affects skeletal muscle mitochondria comparable to pressure overload-induced heart failure. *J Cell Mol Med* 2020; **24**: 6741–6749.
9 Jørgensen T, Grunnet N, Quistorff B. One-year high fat diet affects muscle- but not brain mitochondria. *J Cereb Blood Flow Metab* 2015; **35**: 943–950.
10 Yang XX, Wang X, Shi TT, *et al*. Mitochondrial dysfunction in high-fat diet-induced nonalcoholic fatty liver disease: the alleviating effect and its mechanism of Polygonatum kingianum. *Biomed Pharmacother* 2019; **117**: 109083.
11 Cole MA, Murray AJ, Cochlin LE, *et al*. A high fat diet increases mitochondrial fatty acid oxidation and uncoupling to decrease efficiency in rat heart. *Basic Res Cardiol* 2011; **106**: 447–457.
12 Pengrattanachot N, Cherngwelling R, Jaikumkao K, *et al*. Atorvastatin attenuates obese-induced kidney injury and impaired renal organic anion transporter 3 function through inhibition of oxidative stress and inflammation. *Biochim Biophys Acta Mol Basis Dis* 2020; **1866**: 165741.
13 Depre C, Vanoverschelde JL, Taegtmeyer H. Glucose for the heart. *Circulation* 1999; **99**: 578–588.
14 Jensen J, Rustad PI, Kolnes AJ, Lai YC. The role of skeletal muscle glycogen breakdown for regulation of insulin sensitivity by exercise. *Front Physiol* 2011; **2**: 112.

doi: 10.3164/jcbn.22-73

15 Singh R, Letai A, Sarosiek K. Regulation of apoptosis in health and disease: the balancing act of BCL-2 family proteins. *Nat Rev Mol Cell Biol* 2019; **20**: 175–193.
16 Klionsky DJ, Abdel-Aziz AK, Abdelfatah S, *et al*. Guidelines for the use and interpretation of assays for monitoring autophagy (4th edition). *Autophagy* 2021; **17**: 1–382.
17 Goldberg J, Currais A, Prior M, *et al*. The mitochondrial ATP synthase is a shared drug target for aging and dementia. *Aging Cell* 2018; **17**: e12715.
18 Wilde L, Roche M, Domingo-Vidal M, *et al*. Metabolic coupling and the Reverse Warburg Effect in cancer: implications for novel biomarker and anticancer agent development. *Semin Oncol* 2017; **44**: 198–203.
19 Gai Z, Wang T, Visentin M, Kullak-Ublick GA, Fu X, Wang Z. Lipid accumulation and chronic kidney disease. *Nutrients* 2019; **11**: 722.
20 Dixon AE, Peters U. The effect of obesity on lung function. *Expert Rev Respir Med* 2018; **12**: 755–767.
21 Brock JM, Billeter A, Müller-Stich BP, Herth F. Obesity and the lung: what we know today. *Respiration* 2020; **99**: 856–866.
22 Lian CY, Zhai ZZ, Li ZF, Wang L. High fat diet-triggered non-alcoholic fatty liver disease: a review of proposed mechanisms. *Chem Biol Interact* 2020; **330**: 109199.
23 Monteiro R, Azevedo I. Chronic inflammation in obesity and the metabolic syndrome. *Mediators Inflamm* 2010; **2010**: 289645.
24 Duan Y, Zeng L, Zheng C, *et al*. Inflammatory links between high fat diets and diseases. *Front Immunol* 2018; **9**: 2649.
25 Dhibi M, Brahmi F, Mnari A, *et al*. The intake of high fat diet with different trans fatty acid levels differentially induces oxidative stress and non alcoholic fatty liver disease (NAFLD) in rats. *Nutr Metab (Lond)* 2011; **8**: 65.
26 Tong M, Saito T, Zhai P, *et al*. Mitophagy is essential for maintaining cardiac function during high fat diet-induced diabetic cardiomyopathy. *Circ Res* 2019; **124**: 1360–1371.
27 Chen D, Li X, Zhang L, Zhu M, Gao L. A high-fat diet impairs mitochondrial biogenesis, mitochondrial dynamics, and the respiratory chain complex in rat myocardial tissues. *J Cell Biochem* 2018; **119**: 9602.
28 Vásquez-Trincado C, García-Carvajal I, Pennanen C, *et al*. Mitochondrial dynamics, mitophagy and cardiovascular disease. *J Physiol* 2016; **594**: 509–525.
29 Adeosun SO, Gordon DM, Weeks MF, *et al*. Loss of biliverdin reductase-A promotes lipid accumulation and lipotoxicity in mouse proximal tubule cells. *Am J Physiol Renal Physiol* 2018; **315**: F323–F331.
30 Chandhok G, Lazarou M, Neumann B. Structure, function, and regulation of mitofusin-2 in health and disease. *Biol Rev Camb Philos Soc* 2018; **93**: 933–949.
31 Dai W, Jiang L. Dysregulated mitochondrial dynamics and metabolism in obesity, diabetes, and cancer. *Front Endocrinol (Lausanne)* 2019; **10**: 570.
32 Schrepfer E, Scorrano L. Mitofusins, from mitochondria to metabolism. *Mol Cell* 2016; **61**: 683–694.
33 Putti R, Migliaccio V, Sica R, Lionetti L. Skeletal muscle mitochondrial bioenergetics and morphology in high fat diet induced obesity and insulin resistance: focus on dietary fat source. *Front Physiol* 2016; **6**: 426.
34 Zorzano A, Hernández-Alvarez MI, Palacín M, Mingrone G. Alterations in the mitochondrial regulatory pathways constituted by the nuclear co-factors PGC-1alpha or PGC-1beta and mitofusin 2 in skeletal muscle in type 2 diabetes. *Biochim Biophys Acta* 2010; **1797**: 1028–1033.
35 Gastaldi G, Russell A, Golay A, *et al*. Upregulation of peroxisome proliferator-activated receptor gamma coactivator gene (PGC1A) during weight loss is related to insulin sensitivity but not to energy expenditure. *Diabetologia* 2007; **50**: 2348–2355.
36 Mingrone G, Manco M, Calvani M, Castagneto M, Naon D, Zorzano A. Could the low level of expression of the gene encoding skeletal muscle mitofusin-2 account for the metabolic inflexibility of obesity? *Diabetologia* 2005; **48**: 2108–2114.
37 Bach D, Naon D, Pich S, *et al*. Expression of Mfn2, the Charcot-Marie-Tooth neuropathy type 2A gene, in human skeletal muscle: effects of type 2 diabetes, obesity, weight loss, and the regulatory role of tumor necrosis factor alpha and interleukin-6. *Diabetes* 2005; **54**: 2685–2693.
38 Bach D, Pich S, Soriano FX, *et al*. Mitofusin-2 determines mitochondrial network architecture and mitochondrial metabolism. A novel regulatory mechanism altered in obesity. *J Biol Chem* 2003; **278**: 17190–17197.
39 Houzelle A, Jörgensen JA, Schaart G, *et al*. Human skeletal muscle mitochondrial dynamics in relation to oxidative capacity and insulin sensitivity. *Diabetologia* 2021; **64**: 424–436.
40 Mancini G, Pirruccio K, Yang X, Blüher M, Rodeheffer M, Horvath TL. Mitofusin 2 in mature adipocytes controls adiposity and body weight. *Cell Rep* 2019; **26**: 2849–2858.e4.
41 Bean C, Audano M, Varanita T, *et al*. The mitochondrial protein Opa1 promotes adipocyte browning that is dependent on urea cycle metabolites. *Nat Metab* 2021; **3**: 1633–1647.
42 Diaz B, Fuentes-Mera L, Tovar A, *et al*. Saturated lipids decrease mitofusin 2 leading to endoplasmic reticulum stress activation and insulin resistance in hypothalamic cells. *Brain Res* 2015; **1627**: 80–89.
43 Stacchiotti A, Favero G, Giugno L, *et al*. Mitochondrial and metabolic dysfunction in renal convoluted tubules of obese mice: protective role of melatonin. *PLoS One* 2014; **9**: e111141.
44 Lucas E, Vila-Bedmar R, Arcones AC, *et al*. Obesity-induced cardiac lipid accumulation in adult mice is modulated by G protein-coupled receptor kinase 2 levels. *Cardiovasc Diabetol* 2016; **15**: 155.
45 Elezaby A, Sverdlov AL, Tu VH, *et al*. Mitochondrial remodeling in mice with cardiomyocyte-specific lipid overload. *J Mol Cell Cardiol* 2015; **79**: 275–283.
46 Tsushima K, Bugger H, Wende AR, *et al*. Mitochondrial reactive oxygen species in lipotoxic hearts induce post-translational modifications of AKAP121, DRP1, and OPA1 that promote mitochondrial fission. *Circ Res* 2018; **122**: 58–73.
47 Chen CY, Li SJ, Wang CY, Mersmann HJ, Ding ST. The impact of DRP1 on myocardial fibrosis in the obese minipig. *Eur J Clin Invest* 2020; **50**: e13204.
48 Lionetti L, Mollica MP, Donizzetti I, *et al*. High-lard and high-fish-oil diets differ in their effects on function and dynamic behaviour of rat hepatic mitochondria. *PLoS One* 2014; **9**: e92753.
49 Koncsos G, Varga ZV, Baranyai T, *et al*. Diastolic dysfunction in prediabetic male rats: role of mitochondrial oxidative stress. *Am J Physiol Heart Circ Physiol* 2016; **311**: H927–H943.
50 Enos RT, Velázquez KT, Murphy EA. Insight into the impact of dietary saturated fat on tissue-specific cellular processes underlying obesity-related diseases. *J Nutr Biochem* 2014; **25**: 600–612.
51 Yang C, Aye CC, Li X, Diaz Ramos A, Zorzano A, Mora S. Mitochondrial dysfunction in insulin resistance: differential contributions of chronic insulin and saturated fatty acid exposure in muscle cells. *Biosci Rep* 2012; **32**: 465–478.
52 Holloway GP, Perry CG, Thrush AB, *et al*. PGC-1alpha's relationship with skeletal muscle palmitate oxidation is not present with obesity despite maintained PGC-1alpha and PGC-1beta protein. *Am J Physiol Endocrinol Metab* 2008; **294**: E1060–E1069.
53 Hsu WH, Lee BH, Pan TM. Leptin-induced mitochondrial fusion mediates hepatic lipid accumulation. *Int J Obes (Lond)* 2015; **39**: 1750–1756.
54 Xu J, Cao K, Li Y, *et al*. Bitter gourd inhibits the development of obesity-associated fatty liver in C57BL/6 mice fed a high-fat diet. *J Nutr* 2014; **144**: 475–483.
55 Rashid K, Bhattacharya S, Sil PC. Protective role of D-saccharic acid-1,4-lactone in alloxan induced oxidative stress in the spleen tissue of diabetic rats is mediated by suppressing mitochondria dependent apoptotic pathway. *Free Radic Res* 2012; **46**: 240–252.
56 Zorzano A, Sebastián D, Segalés J, Palacín M. The molecular machinery of mitochondrial fusion and fission: an opportunity for drug discovery? *Curr Opin Drug Discov Devel* 2009; **12**: 597–606.
57 Pich S, Bach D, Briones P, *et al*. The Charcot-Marie-Tooth type 2A gene product, Mfn2, up-regulates fuel oxidation through expression of OXPHOS system. *Hum Mol Genet* 2005; **14**: 1405–1415.
58 Alavi MV, Fuhrmann N. Dominant optic atrophy, OPA1, and mitochondrial quality control: understanding mitochondrial network dynamics. *Mol Neurodegener* 2013; **8**: 32.
59 Del Dotto V, Carelli V. Dominant optic atrophy (DOA): modeling the kaleidoscopic roles of OPA1 in mitochondrial homeostasis. *Front Neurol* 2021; **12**: 681326.
60 Pereira RO, Olvera AC, Marti A, *et al*. OPA1 regulates lipid metabolism and cold-induced browning of white adipose tissue in mice. *Diabetes* 2022; **71**: 2572–2583.
61 Fealy CE, Mulya A, Lai N, Kirwan JP. Exercise training decreases activation of the mitochondrial fission protein dynamin-related protein-1 in insulin-resistant human skeletal muscle. *J Appl Physiol (1985)* 2014; **117**: 239–245.
62 Santos-Alves E, Marques-Aleixo I, Rizo-Roca D, *et al*. Exercise modulates

liver cellular and mitochondrial proteins related to quality control signaling. *Life Sci* 2015; **135**: 124–130.
63 Gan KX, Wang C, Chen JH, Zhu CJ, Song GY. Mitofusin-2 ameliorates high-fat diet-induced insulin resistance in liver of rats. *World J Gastroenterol* 2013; **19**: 1572–1581.
64 Ding Y, Gao H, Zhao L, Wang X, Zheng M. Mitofusin 2-deficiency suppresses cell proliferation through disturbance of autophagy. *PLoS One* 2015; **10**: e0121328.
65 Zorzano A. Regulation of mitofusin-2 expression in skeletal muscle. *A ppl Physiol Nutr Metab* 2009; **34**: 433–439.
66 Quirós PM, Ramsay AJ, López-Otín C. New roles for OMA1 metalloprotease: from mitochondrial proteostasis to metabolic homeostasis. *Adipocyte* 2013; **2**: 7–11.

doi: 10.3164/jcbn.22-73